ACS Photonics

Open Access

pubs.acs.org/journal/apchd5

Article

Structured Excitation Energy Transfer: Tracking Exciton Diffusion below Sunlight Intensity

Guillermo D. Brinatti Vazquez,* Giulia Lo Gerfo Morganti, Cvetelin Vasilev, C. Neil Hunter, and Niek F. van Hulst*

Cite This: *ACS Photonics* 2024, 11, 1318–1326

Read Online

ACCESS | Metrics & More | Article Recommendations

ABSTRACT: With the increasing demand for new materials for light-harvesting applications, spatiotemporal microscopy techniques are receiving increasing attention as they allow direct observation of the nanoscale diffusion of excitons. However, the use of pulsed and tightly focused laser beams generates light intensities far above those expected under sunlight illumination, leading to photodamage and nonlinear effects that seriously limit the accuracy and applicability of these techniques, especially in biological or atomically thin materials. In this work, we present a novel spatiotemporal microscopy technique that exploits structured excitation in order to dramatically decrease the excitation intensity, up to 10,000-fold when compared with previously reported spatiotemporal photoluminescence microscopy experiments. We tested our method in two different systems, reporting the first exciton diffusion measurement at illumination conditions below sunlight, both considering average power and peak exciton densities in an organic photovoltaic sample (Y6), where we tracked the excitons for up to five recombination lifetimes. Next, nanometer-scale energy transport was directly observed for the first time in both space and time in a printed monolayer of the light-harvesting complex 2 from purple bacteria.

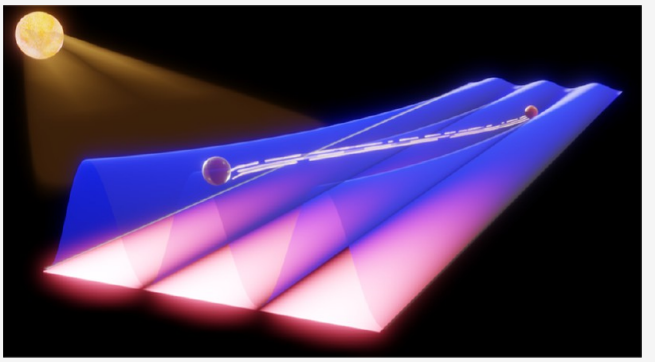

KEYWORDS: *spatiotemporal, exciton, diffusion, light-harvesting, nanoscale transport, sunlight*

INTRODUCTION

Tracking energy flow on the nanoscale has become fundamental for the development of novel technological devices and materials as well as for fundamental research in biology and chemistry. In particular, exciton transport received increasing attention[1] since the advent of new high-performance semiconductors for light harvesting and photonic applications, such as perovskites[2] and transition metal dichalcogenides (TMDs).[3] In chemistry, the transfer of energy between two molecules is usually referred to as excitation energy transfer (EET), which has been investigated extensively, for example, in the process of photosynthesis.[4,5]

Visualization of nanoscale energy transport is a challenging task, requiring high resolution in both space and time, as exciton recombination lifetimes are usually in the picosecond to nanosecond range and transport lengths are on the order of tens of nanometers. To achieve this, ultrafast lasers and high-resolution microscopy have been combined in a variety of techniques that exploit transient absorption (TA)[6−9] or photoluminescence[10] (PL) to report on exciton transport.

Despite the success of these techniques, they require laser intensities that are many orders of magnitude above sunlight (operando) conditions. This has two major drawbacks: first, photodamage limits the application of spatiotemporal microscopy, especially in biological and atomically thin samples. Second, high exciton densities lead to the presence of many-body effects, such as singlet−singlet annihilation (SSA), usually causing an overestimation of the diffusion coefficients.[11−13] These limitations apply particularly to methods based on TA,[14,15] as they rely on a nonlinear contrast mechanism.[16] Alternatively, as PL is linear, point-excitation spatiotemporal PL (PE) microscopy is the chosen technique when low fluences are required. This method has proven useful in studying different materials, including TMDs,[17,18] perovskites,[19−21] quantum-dots solids,[22] and many others.[10,11,23]

As its name suggests, PE microscopy uses a diffraction-limited spot to excite the sample, and the diffusion properties are obtained by performing spatiotemporal maps of the emitted PL. This is achieved by a spatially displaced confocal

Received: January 2, 2024
Revised: February 9, 2024
Accepted: February 12, 2024
Published: February 22, 2024

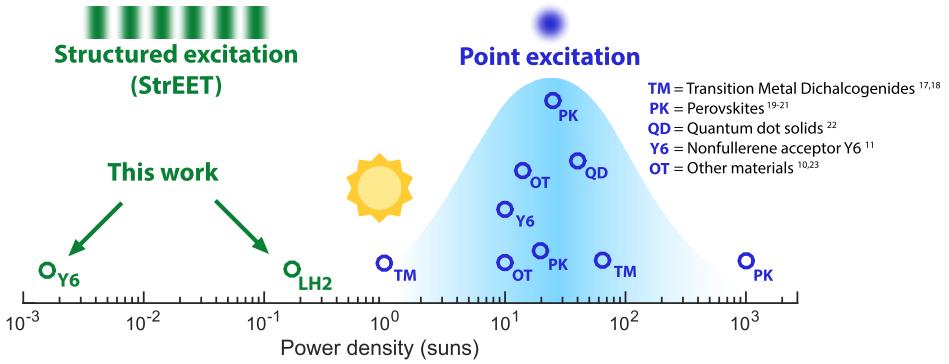

Figure 1. Excitation power densities needed for StrEET (this work) and previously reported point-excitation spatiotemporal microscopy experiments in units of sunlight intensity (1 sun = 0.1 W/cm^2). Using the point-excitation technique, most samples required between 10 and 100 solar intensities.

detection, where a small pinhole is scanned across the excitation beam and the collected light is detected in a time-correlated single photon counting (TCSPC) scheme[10] or using a streak camera.[24] As a result, two-dimensional (2D) maps (photon arrival time vs pump-detection relative distance) are acquired, where diffusion is directly observed as a spatial broadening of the exciton population whose squared width grows linearly with time.[25] As diffusion lengths are usually in the order of tens of nanometers[26] (far below the diffraction limit), the fitting of a broadened point spread function (PSF) model is required, usually a Gaussian. The fitting dramatically increases the spatial accuracy, allowing for the detection of such small variations in the PL emission.

Nevertheless, as very small broadening must be detected, tightly focused beams and high signal-to-noise ratios (SNR) are necessary, again requiring an increase in the excitation fluence. Moreover, small differences between the real PSF and the fitted model may lead to signal artifacts and inaccuracies. As shown in Figure 1 (and using the intensity of sunlight at the Earth's surface, roughly 0.1 W/cm^2, as a reference), a literature review shows that most PE microscopy measurements were performed with a power density in the range between 10 and 100 solar intensities, with the lowest reported close to one sun. This means that the goal of performing measurements under sunlight conditions has still not been achieved for most samples.

A recent study used PE microscopy to investigate the effect of laser fluence on exciton diffusion in the nonfullerene acceptor Y6 (a promising organic photovoltaic material for the next-generation solar energy harvesting devices[27−29]) and proposed a method for uncoupling the SSA effect on the diffusion coefficient.[11] Nevertheless, this approach requires a fluence dependence study, together with a numerical fit of an SSA model.

Here, we present structured EET (StrEET) microscopy, a novel method for spatiotemporally resolved EET measurements that exploits structured excitation to achieve measurements at extremely low light levels. This is accomplished by an increase in the sensing area, which is interrogated in a parallel fashion, allowing a fluence reduction by up to 10^4-fold when compared to point-excitation (as shown in Figure 1). Additional benefits of the method are that no PSF nor lifetime fitting is required, as the transport information is obtained from a simple computation between two time-resolved PL traces, and increased accuracy, as the spatial scale is given by the excitation structure. Details of the technique are presented, followed by experimental results. We show ultralow fluence measurements (below solar power densities) in two different samples. In the first, we use the nonfullerene acceptor Y6, where we demonstrate the relevance of measuring at low fluences to avoid SSA contributions to the diffusivity, and in the second we use a monolayer[30] of light-harvesting complex 2 (LH2 of purple photosynthetic bacteria[5,31]). LH2 is a fragile biological antenna system where photobleaching and SSA[32,33] are relevant at relatively low pump fluences and, thus, reducing the fluence is of vital importance for the experiment. Although evidence of transport was previously presented for LH2-based systems,[33,34] our experiment is, to our knowledge, the first to track the diffusion of excitons in both space and time.

STREET MICROSCOPY

In this section, we describe the method and present the mathematical formulation that allows for the retrieval of the diffusion properties using StrEET microscopy.

As stated previously, the goal of the method is to reduce the excitation fluence by redistributing the pump light over a larger area of the sample. If the total number of incident photons is kept constant, this leads to a reduction of the exciton density without a loss of SNR, as the total number of detected photons is also conserved. In any case, high spatial frequency excitation is required to retrieve spatial information, so we used a sine-wave pattern with a period close to the diffraction limit. Conceptually, the method exploits the reduction of the modulation amplitude of the periodic excitation caused by diffusion, as illustrated in Figure 2a. As the excitons diffuse, they migrate following the concentration gradient (peaks to valleys of the excitation), leading to a washing out of the periodic structure.

This idea is also at the heart of transient grating spectroscopy (TGS),[35,36] where the spatial distribution of the exciton population acts as a diffraction grating for a probe beam, whose diffraction efficiency reports on the modulation contrast of the grating. Here two important differences to TGS should be noted: first, TGS is a pump−probe technique, meaning that a nonlinear signal is being measured, whereas PL is a linear signal, which allows for a large reduction of the excitation fluence. Second, the low fluence is combined with photon counting, and the pump pulse has to produce only a few excitations, which are distributed over an area as large as 40 μm in diameter. This means that the exciton population hardly resembles a diffraction grating at any time. Indeed, the spatial information in StrEET microscopy is not recovered

https://doi.org/10.1021/acsphotonics.4c00004
ACS Photonics 2024, 11, 1318−1326

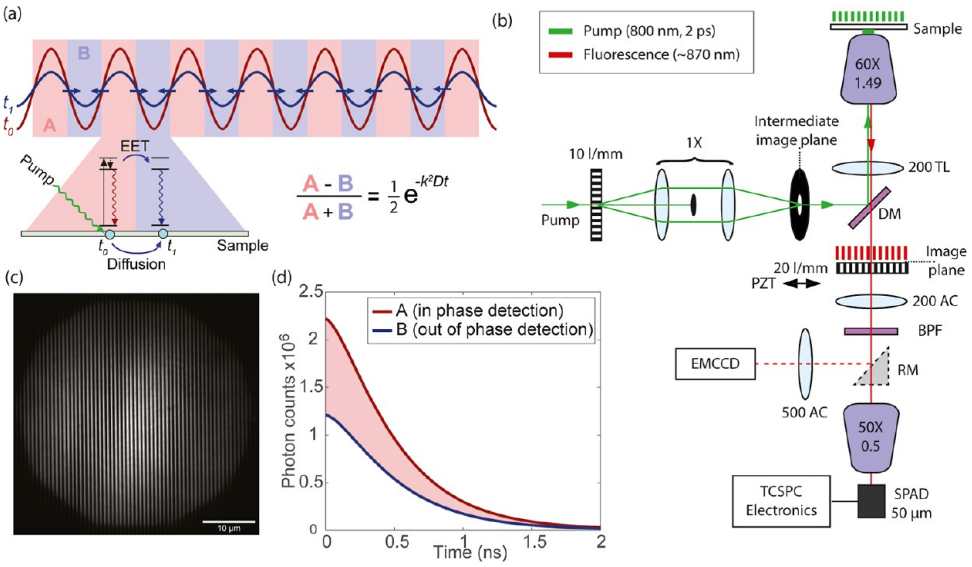

Figure 2. StrEET microscopy method and experimental setup. (a) Representation of the PL spatial dependence under sine-wave excitation for two different times. Shaded regions represent the two areas selected by the detection mask. A zoom shows how an exciton created in region A can emit a PL photon there or in region B after diffusing, leading to different PL dynamics. (b) Experimental setup, representing the pump and PL beam paths through the microscope. A transmission mask is used to select the two areas of interest. (c) EMCCD image of a representative sample showing the structured excitation pattern. (d) Time-resolved PL traces for the two positions of the transmission mask (on a Y6 sample), whose difference (shaded region) contains the transport information.

from a collective modulation of the refractive index of the sample, but from a statistical average of the individual emission positions. To achieve this, a periodic transmission mask is introduced in the detection path, to selectively block the photons emitted from either the peaks or the valleys of the excitation. The emission of all the excited area (after the mask) is integrated into a single-pixel avalanche detector. This results in two individual time-resolved PL traces (corresponding to the two selected areas), from where we calculate the diffusion properties of the sample without the need for any fitting.

To formally describe this scheme, we start by considering a short light pulse that excites our sample with a sine-wave spatial dependence in one direction. Because of the interaction with the incident electric field, an exciton population is created whose location probability reproduces the same spatial structure as the excitation. After this, the system will start evolving due to two major effects: diffusion and recombination. For an exciton population N of characteristic recombination time τ experiencing isotropic, in-plane diffusion, the differential equation describing the evolution of the system takes the form[37]

$$\frac{\partial N}{\partial t}(\vec{r}, t) = D\nabla^2 N(\vec{r}, t) - \frac{1}{\tau}N(\vec{r}, t) \tag{1}$$

where $\vec{r} = (x,y)$ and t are the spatial and temporal degrees of freedom and D is the diffusivity. Thus, for a periodic sine-like excitation, we can write the exciton population at time zero (shortly after the interaction with the laser) as

$$N(\vec{r}, t = 0) = \frac{N_o}{2}(1 + \cos kx) \tag{2}$$

where k is the excitation spatial frequency and N_o is a scale factor which depends on the absorption cross-section and the laser parameters. The evolution of this initial state under eq 1 is

$$N(\vec{r}, t) = \frac{N_o}{2}e^{-t/\tau}(1 + e^{-k^2Dt}\cos kx) \tag{3}$$

Because of the linearity of eq 1, expression 3 has the same spatial frequency components present in the initial population, and only the amplitude of each term changes over time. Indeed, we can see that the CW component contains information only on the recombination lifetime τ, while the oscillatory term (at spatial frequency k) is affected by both recombination and transport. Thus, diffusion information can be isolated by computing a ratio between these two spatial frequency components. To achieve this, we need to spatially demodulate our PL signal to retrieve the individual amplitudes of each term. To do so, the emission from the sample is imaged on a transmission mask with identical periodicity. The PL intensity distribution I after the mask is then obtained by multiplication of the transmission function as

$$I = I_o e^{-t/\tau}(1 + e^{-k^2Dt}\cos kx)(1 + \cos(kx + \varphi)) \tag{4}$$

where I_o is a proportionality factor related to N_o by the emission properties of the sample and φ is the relative phase between the excitation and the transmission mask periodicities. If we expand this expression, we will find terms at spatial frequencies 0, k, and $2k$. As we want to integrate all of the PL in a single point detector, only the CW frequency component will contribute, as the other two will average to zero. From these considerations, we find that the integrated signal in our detector S can be expressed as

$$S = S_o e^{-t/\tau}\left(1 + \frac{1}{2}e^{-k^2Dt}\cos\varphi\right) \tag{5}$$

where S_o is a proportionality constant related to I_o by the properties of the optics and the detector. Choosing appropriate values of φ allows us to isolate the transport and recombination contributions. It is easy to see that the maximum and minimum values of transmission will occur

https://doi.org/10.1021/acsphotonics.4c00004
ACS Photonics 2024, 11, 1318−1326

when the mask is in phase and out of phase, respectively, with respect to the excitation. We define these two signals as A and B (obtained by evaluating $\varphi_A = 0$ and $\varphi_B = \pi$ in eq 5). These are the only two experimental measurements required to retrieve the diffusivity of our sample. First, we simply need to realize that $A - B$ is the amplitude of our spatial modulation, i.e., the one containing both D and τ information. Second, $A + B$ is twice the average value, i.e., the CW term, containing only τ. We can also understand $A + B$ as being the integrated signal without using the periodic mask in detection where the diffusion information is averaged to zero. It is then easy to see that

$$\frac{A - B}{A + B} = \frac{1}{2}e^{-k^2 Dt} \tag{6}$$

where the dependence on τ is no longer present. From this expression, we only need to accurately know k, the excitation spatial frequency, to get D. Unsurprisingly, this expression is the impulse response function of the diffusion equation in the spatial frequency domain. As higher frequencies decay faster than the lower ones, the sensitivity of the method is maximized when the excitation period is close to the diffraction limit. In contrast, point-excitation requires a broad band of spatial frequencies to achieve tight focusing, of which the lower part carries little information, as their associated decay times are much longer than the recombination lifetime. As a result, StrEET recovers the same information with reduced fluence and leads to a much easier interpretation of the data. Also, the use of the demodulation mask allows encoding the spatial information into intensity variations, increasing the SNR, and eliminates the need for Gaussian fitting to track the excitation expansion. Moreover, accuracy is enhanced, as the spatial scale is defined purely by the excitation period, which is produced by a high-precision diffraction grating, leading to reduced calibration errors. The only trade-off for these advantages is that the diffusion information is averaged over the whole excitation area, making the method suitable for relatively homogeneous samples. It should be noted that also point-excitation methods still impose some homogeneity constraints, as the diffusion is required to be constant on a scale a few times larger than the excitation full-width half-maximum to accurately fit a Gaussian model. This leads to an effective spatial resolution (meaning the ability to resolve spatial changes in the transport properties of the sample) in the order of a few microns.

To visualize the transport of energy, previous studies[20,21] define the mean square displacement (MSD) as the variance of the impulse response function of the diffusion equation in the spatial domain. For a direct comparison, we can obtain the same information from eq 6, leading to

$$\mathrm{MSD}(t) = -\frac{2}{k^2}\log\left(\frac{A - B}{A + B}\right) \propto 2Dt \tag{7}$$

the slope of which is proportional to the diffusivity. This equation highlights the fact that the method needs only two spatial measurements (in contrast to the many required to accurately fit a Gaussian PSF model) and that no fitting is required to track the diffusion.

As A and B are the extrema of eq 5, small variations in the relative phase between the excitation and the demodulation mask will only cause a signal variation that is proportional to the square of the positioning error, making the method very robust to small misalignments. In fact, because of the normalization, the technique requires only a phase difference of π between A and B to isolate the diffusion contribution. For the case of $\phi_A \neq 0$ and $\phi_B \neq \pi$ but $\phi_B - \phi_A = \pi$, eq 6 holds with a proportionality factor smaller than 1/2 (which relates to the cosine value at ϕ_A) that becomes a constant offset when the logarithm is evaluated in expression 7, the slope of which still reports on the diffusivity. The same argument holds for an imperfect sine-like illumination, which also reduces the 1/2 contrast factor in eq 6. Taking all of these considerations into account, positioning accuracy on the order of one micron is required, which is easily achieved with a piezoelectric actuator. For accurate positioning of the detection mask, a calibration measurement is performed prior to the diffusion measurements, where fluorescence is collected while scanning the actuator position. From this scan, the locations corresponding to ϕ_A and ϕ_B are precisely identified as the maximum and minimum of the fluorescence signal.

Equation 1 assumes that the interaction between excitons is negligible. This is not the case for high excitation fluences, where many-body effects such as SSA are often relevant. To account for this, a quadratic term of the form $-\gamma(t)N^2$ should be included in eq 1, where $\gamma(t)$ is a function that accounts for the annihilation rate.[38] The solution to this nonlinear equation becomes nonanalytical and dependent on the initial fluence. The use of the linear solution when nonlinearities are present leads to an overestimation of the diffusion coefficients, which can be understood as arising from a distortion of the Gaussian profiles in the point-excitation method or from an accelerated modulation amplitude decay in the one proposed here. In situations where SSA cannot be neglected, a numerical fit of the full model [including the quadratic SSA term $-\gamma(t)N^2$] can still be performed, as proposed in previous point-scanning TA measurements,[6] where γ was assumed to be constant. Nevertheless, the drastic reduction in fluence achieved by StrEET allows SSA to be completely ruled out in most cases, leading to a simpler and more accurate data analysis.

The experimental setup used for the measurement of diffusion using StrEET microscopy is shown in Figure 2b and thoroughly described in the Methods section. Briefly, a diffraction grating and a high NA microscope objective are used to generate a high-frequency structured illumination in the sample. The PL emission is collected by the same objective, spectrally separated, and imaged on a transmission mask of the same period as the excitation, mounted on a piezoelectric actuator. The transmitted light is then integrated into a single-photon avalanche detector (SPAD) for TCSPC. The overall magnification is 1.2× sample to detector, limiting the maximum collection area to about 42 μm in diameter for a 50 μm diameter SPAD. For this particular situation, the fluence reduction compared to a diffraction-limited point-excitation setup is greater than 12,000 times.

Figure 2c shows the PL arising from the periodic excitation of a homogeneous, 50 nm thick Y6 film. Two typical time-resolved PL traces corresponding to mask positions A and B (peaks and valleys) are shown in Figure 2d. There, we can see that the difference between the two curves (pink shading), which contain the diffusion information, decreases with time, as expected from eq 6. A typical measurement is performed by acquiring these two traces in an alternated way and for a relatively short integration time (around 10 s) to avoid saturation of the TCSPC electronics and to minimize the

https://doi.org/10.1021/acsphotonics.4c00004
ACS Photonics 2024, 11, 1318−1326

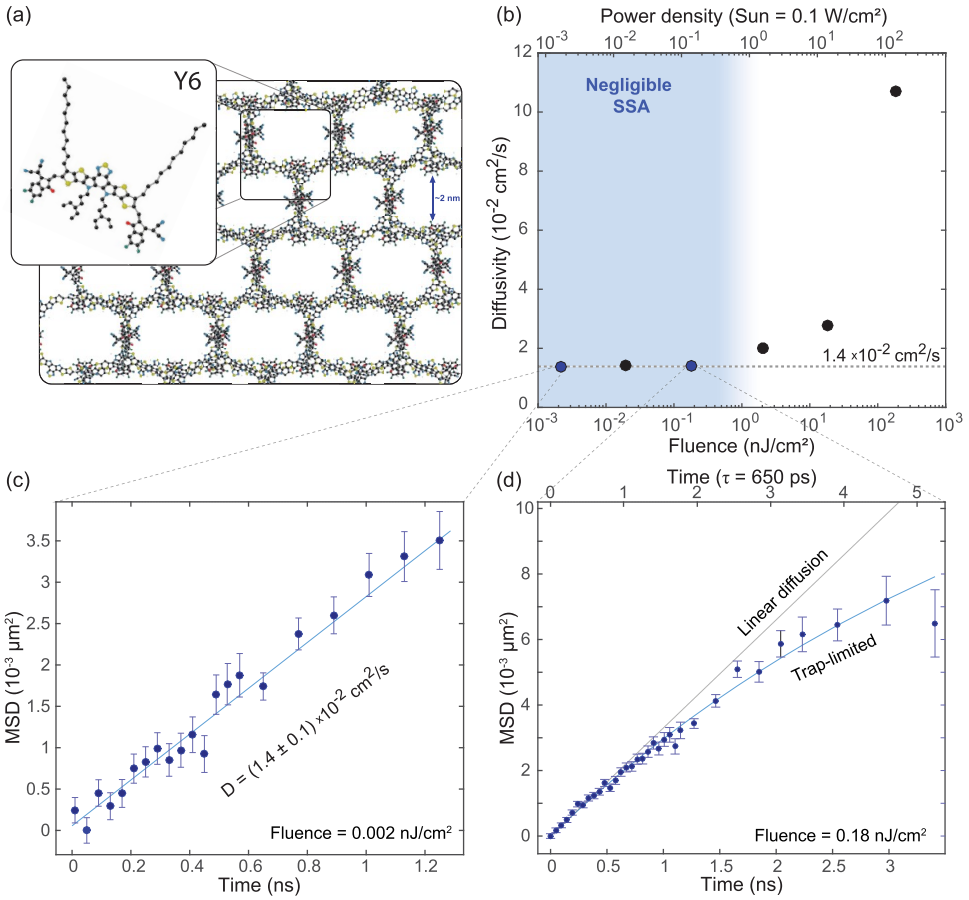

Figure 3. Results of the StrEET microscopy experiment in a Y6 sample. (a) Y6 molecule and crystalline lattice.[39] (b) Fitted diffusivity against excitation fluence, showing apparent increase at high fluences due to the presence of SSA. (c) MSD measurement for the lowest fluence of 0.002 nJ/cm^2 and linear fit for diffusivity estimation. (d) MSD at 0.18 nJ/cm^2 for a longer time scale. Sublinearity of the MSD evidence the presence of trap states.

effects of bleaching. The desired SNR is then achieved by iteration of this process.

RESULTS AND DISCUSSION

We start by characterizing the performance of the method in a Y6 sample, as illustrated in Figure 3. For this purpose, a fluence dependence study was performed, covering 5 orders of magnitude from 0.002 nJ/cm^2 up to 190 nJ/cm^2. Compared to the solar power density, this corresponds to 10^{-3} up to 100 solar intensities. Note that, as shown in Figure 1, most PE microscopy measurements are performed in the range between 10 and 100 solar intensities.

The results of these experiments are listed in Figure 3. For every fluence, TCSPC traces are acquired for the detection regions A and B and, after this, MSD is calculated using expression 7. From each MSD plot, diffusion is obtained from the slope of a linear fit constrained to the first lifetime of the PL signal (around 650 ps). In Figure 3b, the resulting diffusivities are plotted against fluence (and sun intensity in the upper axis), showing a constant value for fluences smaller than 1 nJ/cm^2, resulting in $D = (1.41 \pm 0.03) \times 10^{-2}$ cm^2/s (2% relative error) at a fluence of 0.18 nJ/cm^2, and corresponding to a diffusion length of $\sqrt{2D\tau} = 43$ nm. In Figure 3c, we show the MSD signal at the lowest fluence of 0.002 nJ/cm^2, where the linear fit (light blue) results in $D = (1.4 \pm 0.1) \times 10^{-2}$ cm^2/s (7% relative error). At higher fluences, the diffusivity apparently increases, as expected from SSA. This effect is particularly important in the range where PE microscopy experiments are usually performed, where overestimations of the diffusivity of up to *a* factor of 10 are observed.

A previous study on the same sample using the point-excitation strategy[11] also reported an important SSA annihilation effect. In this work, values of $D = (2.0 \pm 0.6) \times 10^{-2}$ cm^2/s and $D = (2.3 \pm 0.3) \times 10^{-2}$ cm^2/s are reported for different fitting models at a fluence of 13 nJ/cm^2 (5 excitations per pulse), together with a numerical solution to the differential equation including a quadratic SSA term, resulting in an estimated diffusivity of $D = (1.7 \pm 0.3) \times 10^{-2}$ cm^2/s. These values are close to the ones found here and might still overestimate diffusivities due to SSA, as our results suggest. Notice that the estimations provided by the point-excitation technique require various levels of mathematical abstraction and fitting, such as PSF fitting for the width extraction and 2D numerical modeling for the low fluence extrapolation. On the other hand, our structured excitation approach retrieves the exciton MSD without any fitting, and ultralow fluence measurements completely rule out nonlinear effects.

Until now, we made use of average power densities to compare with solar intensities, as is usual in literature. Nevertheless, and from the sample point of view, operando conditions are better described by accounting for the steady-state exciton density present in the material under solar illumination. This number is system-dependent, as it is affected by absorption cross sections, recombination lifetime, and

https://doi.org/10.1021/acsphotonics.4c00004
ACS Photonics 2024, 11, 1318−1326

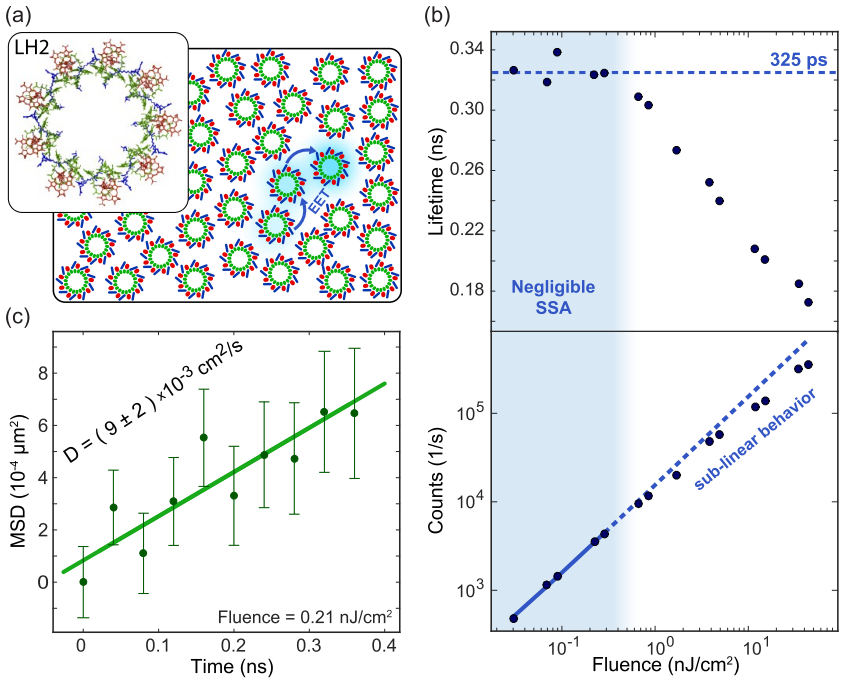

Figure 4. Results of the StrEET microscopy experiment in an LH2 monomolecular layer. (a) Structure of the light-harvesting 2 complex[31] and idealized representation of the distribution of the molecules in the sample (printed monolayer). (b) Fluence dependence study showing the effect of SSA in the exciton lifetime (top) and total PL counts. (c) MSD in an LH2 sample excited at 0.21 nJ/cm^2 from which a diffusivity of $D = (9 \pm 2) \times 10^{-3}$ cm^2/s and a diffusion length of 24 nm are obtained.

spectral overlaps. To see if our particular experiment is below this threshold, we can define the operando-equivalent fluence for a given material and pump wavelength as the fluence at which the peak exciton density is equal to the steady-state density under sunlight. This means that the exciton density during the experiment will be lower than that expected at operation at all times. For Y6 and a laser wavelength of 800 nm this results in an operando-equivalent fluence of 0.023 nJ/cm^2, a much lower threshold than the 1.3 nJ/cm^2 obtained from comparing average intensities. Nevertheless, our measurement at the very low fluence of 0.002 nJ/cm^2 is still 1 order of magnitude below the threshold, making this, to our knowledge, the first direct measurement of the exciton diffusivity below operando illumination conditions, both considering average power density and peak exciton density.

An additional advantage of our method is that as a consequence of increased SNRs, excitons can be tracked for much longer times. In Figure 3d, we show the MSD signal measured at a fluence of 0.18 nJ/cm^2 (below one solar average intensity and the SSA threshold), where the excitons can be tracked up to 3.5 ns, equivalent to 5 exciton lifetimes ($1/e$ decay time). At these long times, we can see that the diffusion equation (dashed line) starts failing to describe the data, which shows a subdiffusive expansion. This kind of behavior was already observed by PE microscopy in tetracene[10] and perovskites,[20,21] but never before in Y6, and it is attributed to the presence of trap states. A homogeneous trap distribution model was proposed[20] to describe this, leading to an exponential saturation of the MSD of the form

$$\mathrm{MSD}(t) = 2\lambda^2(1 - \mathrm{e}^{-Dt/\lambda^2}) \tag{8}$$

where λ is the average trap distance. We can see that for $t \ll \lambda^2/D$ the linear behavior is recovered. By fitting this model (full line), we retrieve an average trap distance of λ = 180 nm, corresponding to a trap density of 3×10^9 cm^{-2}. This shows that StrEET microscopy can provide additional sample information, even at average intensities below sunlight.

In addition to the Y6 characterization shown so far, we present the first spatiotemporal measurement of exciton transport in a printed monolayer of LH2, from purple bacteria. As shown in Figure 4a, these very large biological molecules consist of a hollow cylinder of 18 protein subunits that bind rings of 9 and 18 bacteriochlorophylls (red and green), and a ring of 9 carotenoids (blue).[31] LH2 complexes have a low PL quantum yield and are very easily photobleached under intense excitation, making this a particularly demanding experiment. Again, we observed an apparent fluence-dependent diffusivity, which marked the presence of SSA effects. Because of the reduced number of photons at equal pumping (compared to Y6), the measurement of a full diffusivity versus fluence curve was not a convenient way to determine the appropriate pump levels. Instead, the dependence of the excited state lifetime and the linearity of the total number of counts were used as indicators of the presence of SSA. For this, the PL dynamics were measured without a detection mask to integrate the diffusion contribution to the signal. The resulting PL signal was fitted by a biexponential model. The shortest of the lifetimes is plotted as a function of pump fluence in Figure 4b (top), where it is clearly seen how the decay gets faster with increasing pulse energy, as expected for the additional decay pathway provided by SSA. In the bottom part of Figure 4b, the total number of PL counts is again plotted against fluence, showing a clear sublinear behavior at higher fluences. We can see that SSA effects become negligible below a certain threshold at around 0.3 nJ/cm^2 (shaded region), where the lifetime stabilizes at around 325 ps, and the total counts show a linear dependence. It is also observed that the relative weight of the exponential term plotted in Figure 4b approaches unity

https://doi.org/10.1021/acsphotonics.4c00004
ACS Photonics 2024, 11, 1318−1326

at the low fluence range, resulting in essentially mono-exponential dynamics for fluences below the 0.3 nJ/cm^2 threshold.

We selected a fluence of 0.21 nJ/cm^2 to perform the transport measurements shown in Figure 4c. Even at this low fluence, bleaching is still important, limiting the maximum achievable photon counts. Because of this, five consecutive regions of the sample were averaged to further boost the SNR. In the results shown in Figure 4c, we can clearly identify a linear expansion of the MSD for the first lifetime from where we estimate a diffusivity of $D = (9 \pm 2) \times 10^{-3}$ cm^2/s and, as a consequence, a diffusion length of 24 nm. This value confirms that the exciton is visiting several complexes (each one around 7 nm in diameter) before recombination. In fact, it is exploring an area of 1800 nm^2, that might contain up to 42 LH2 complexes, similar to numbers observed in living samples using SSA.[33] In any case, the transport properties are expected to be strongly dependent on the average distance between the complexes and, thus, a density study is required to address relevant questions on this matter. Anyway, the measurements presented here on a fragile biological sample of molecular thickness demonstrate the power of the method and open the door for new experimental studies on energy transport in photosynthetic membranes.

CONCLUSIONS

We present StrEET microscopy, a novel method that uses structured excitation to measure exciton diffusion in photoluminescent samples using extremely low light levels, reaching 10^4-fold fluence reduction when compared to point-illumination spatiotemporal microscopy methods. StrEET requires only two spatial measurements to track the diffusion of excitons in space and time and without the need of fitting PSF models. The method is by design robust to misalignment and calibration errors, and because of the low fluence requirements, it is particularly suited for samples where nonlinear effects are relevant or where photodamage is a concern.

The performance of the method was evaluated in a Y6 sample, where fluence was reduced down to the pJ/cm^2 level, resulting in the first direct measurement of exciton diffusion below sunlight illumination conditions, considering both average power density and peak exciton density. Because of the increased SNR, we were able to track exciton expansion for up to five recombination lifetimes, observing a subdiffusive behavior at long times, attributed to the presence of trap states.

Additionally, the future possibilities of the technique were illustrated by showing the first direct measurement of exciton transport in a printed monomolecular layer of LH2 complexes, where a diffusion length of 24 nm was determined. This was achieved using a fluence of 0.21 nJ/cm^2, which is again well below solar power densities. We are convinced that StrEET microscopy has the potential to play an important role in the quest for better and more efficient light-harvesting materials by extending the use of spatiotemporal microscopy to samples previously impossible to investigate, and by providing an accurate and more complete characterization of these materials under low light-level operation conditions.

METHODS

StrEET Setup. The experimental setup is depicted in Figure 2b. Short pulses at 800 nm are obtained from a titanium-sapphire oscillator (76 MHz, 150 fs). The pulses are spatially filtered and stretched up to 2 ps using 20 m of a single-mode fused silica optical fiber. After collimation, the beam is sent to an amplitude grating (chrome on glass, 10 lines/mm), which will ultimately be imaged into the sample. An intermediate image is first produced by means of a 1:1 telescope made of two identical 150 mm achromatic lenses. A metallic mask is placed in the Fourier plane of the telescope to block all the diffraction orders other than ±1. An iris is placed in the intermediate image plane to control the excitation area. Light reflects in a long-pass dichroic mirror (DM, Thorlabs DMLP805) and is then imaged in the sample by the main microscope optics (200 TL, Thorlabs TL200A tube lens and Olympus 60× 1.49 NA objective), leading to a sine-wave excitation with a period of 750 nm. PL is collected by the same objective, transmitted by the dichroic mirror, and spectrally filtered using a fluorescence bandpass filter. Another amplitude grating (chrome on glass, 20 lines/mm) is placed in the image plane. The grating is mounted in a piezoelectric actuator (PZT) with a 57 μm total range. The transmitted light is collected by a 200 mm achromatic lens (200 AC) and then imaged in the SPAD detector (MPD-PD050C0E, 50 μm diameter active area, 50 ps temporal resolution) with a long working distance objective (Olympus LMPLFLN 50× 0.5 NA). Time-correlated single photon counting is achieved by feeding the individual photon arrival pulses to a PicoQuant PicoHarp 300 system, together with a reference signal of the pump beam obtained by a fast PIN photodiode. A removable mirror can be placed before the detection objective to direct the fluorescence to an EMCCD camera for sample visualization.

Sample Preparation. Sample preparation is described in detail elsewhere for Y6[11] and LH2.[30] Briefly, 50 nm thick Y6 samples were prepared to start from a solution of Y6 polymer (eflexPV) in chloroform (6 mg/mL), which is spin-coated at 1000 rpm onto a cleaned 0.17 mm thick coverslide. Samples were thermally annealed (50 °C, 3 min) and sealed within a dry nitrogen atmosphere by covering with an additional cover slide held in place using UV adhesive (NOA 73, Norland).

For the LH2 samples, a polydimethylsiloxane stamp was prepared by mixing Sylgard184 silicon elastomer base and curing agents (Dow Corning, ratio 10:1), which is then cast onto a Si master template. The stamp was immersed in a solution of LH2 complexes (15 μM protein in buffer consisting of 20 mM HEPES, 0.03% β-DDM) for five min and subsequently blown dry using Argon. Before the stamping, a 0.17 mm thick coverslide coated with poly-L-lysine was treated with 20 mM dimethyl suberimidate to activate lysine as the cross-linker for amine attachment. The LH2 molecules were printed on the surface by gently placing the stamp on top of the treated substrate for 5 min. Samples were sealed in a dry nitrogen atmosphere to lower the extent of bleaching.

AUTHOR INFORMATION

Corresponding Authors

Guillermo D. Brinatti Vazquez − *ICFO-Institut de Ciencies Fotoniques, The Barcelona Institute of Science and Technology, Castelldefels, Barcelona 08860, Spain;* orcid.org/0000-0003-1921-8029; Email: guillermo.brinatti@icfo.eu

Niek F. van Hulst − *ICFO-Institut de Ciencies Fotoniques, The Barcelona Institute of Science and Technology, Castelldefels, Barcelona 08860, Spain; ICREA-Institució Catalana de Recerca i Estudis Avançats, Barcelona 08010,*

https://doi.org/10.1021/acsphotonics.4c00004
ACS Photonics 2024, 11, 1318−1326

Spain; orcid.org/0000-0003-4630-1776;
Email: niek.vanhulst@icfo.eu

Authors

Giulia Lo Gerfo Morganti − *ICFO-Institut de Ciencies Fotoniques, The Barcelona Institute of Science and Technology, Castelldefels, Barcelona 08860, Spain;* orcid.org/0000-0001-5814-5542

Cvetelin Vasilev − *School of Biosciences, University of Sheffield, Sheffield S10 2TN, U.K.*

C. Neil Hunter − *School of Biosciences, University of Sheffield, Sheffield S10 2TN, U.K.;* orcid.org/0000-0003-2533-9783

Complete contact information is available at: https://pubs.acs.org/10.1021/acsphotonics.4c00004

Notes

The authors declare no competing financial interest.

■ ACKNOWLEDGMENTS

G.D.B.V., G.L.G.M., and N.F.v.H. acknowledge support through the MCIN/AEI projects PID2021-123814OB-I00, TED2021-129241B−I00, the "Severo Ochoa" program for Centres of Excellence in R&D CEX2019-000910-S, Fundacio Privada Cellex, Fundacio Privada Mir-Puig, and the Generalitat de Catalunya through the CERCA program. G.L.G.M. is supported through the MCIN/AEI project PRE2019-091051. N.F.v.H. acknowledges the financial support from the European Commission (ERC Advanced Grant 101054846—FastTrack). This work is part of the ICFO Clean Planet Program supported by Fundació Joan Ribas Araquistain (FJRA). C.N.H. and C.V. gratefully acknowledge funding (BB/V006630/1) from the Biotechnology and Biological Sciences Research Council UK. C.N.H. is also supported by the European Research Council Synergy award 854126.

■ REFERENCES

(1) Ginsberg, N. S.; Tisdale, W. A. Spatially resolved photogenerated exciton and charge transport in emerging semiconductors. *Annu. Rev. Phys. Chem.* **2020**, *71*, 1−30.
(2) Kim, J. Y.; Lee, J.-W.; Jung, H. S.; Shin, H.; Park, N.-G. High-efficiency perovskite solar cells. *Chem. Rev.* **2020**, *120*, 7867−7918.
(3) Manzeli, S.; Ovchinnikov, D.; Pasquier, D.; Yazyev, O. V.; Kis, A. 2D transition metal dichalcogenides. *Nat. Rev. Mater.* **2017**, *2*, 17033−17115.
(4) Şener, M.; Strümpfer, J.; Hsin, J.; Chandler, D.; Scheuring, S.; Hunter, C. N.; Schulten, K. Förster energy transfer theory as reflected in the structures of photosynthetic light-harvesting systems. *ChemPhysChem* **2011**, *12*, 518−531.
(5) Mirkovic, T.; Ostroumov, E. E.; Anna, J. M.; Van Grondelle, R.; Govindjee; Scholes, G. D. Light absorption and energy transfer in the antenna complexes of photosynthetic organisms. *Chem. Rev.* **2017**, *117*, 249−293.
(6) Wan, Y.; Guo, Z.; Zhu, T.; Yan, S.; Johnson, J.; Huang, L. Cooperative singlet and triplet exciton transport in tetracene crystals visualized by ultrafast microscopy. *Nat. Chem.* **2015**, *7*, 785−792.
(7) Zhu, Y.; Cheng, J.-X. Transient absorption microscopy: Technological innovations and applications in materials science and life science. *J. Chem. Phys.* **2020**, *152*, 020901.
(8) Choudhry, U.; Kim, T.; Adams, M.; Ranasinghe, J.; Yang, R.; Liao, B. Characterizing microscale energy transport in materials with transient grating spectroscopy. *J. Appl. Phys.* **2021**, *130*, 231101.
(9) Delor, M.; Weaver, H. L.; Yu, Q.; Ginsberg, N. S. Imaging material functionality through three-dimensional nanoscale tracking of energy flow. *Nat. Mater.* **2020**, *19*, 56−62.
(10) Akselrod, G. M.; Deotare, P. B.; Thompson, N. J.; Lee, J.; Tisdale, W. A.; Baldo, M. A.; Menon, V. M.; Bulović, V. Visualization of exciton transport in ordered and disordered molecular solids. *Nat. Commun.* **2014**, *5*, 3646.
(11) Lo Gerfo M, G.; Bolzonello, L.; Bernal-Texca, F.; Martorell, J.; van Hulst, N. F. Spatiotemporal Mapping Uncouples Exciton Diffusion from Singlet−Singlet Annihilation in the Electron Acceptor Y6. *J. Phys. Chem. Lett.* **2023**, *14*, 1999−2005.
(12) Firdaus, Y.; Le Corre, V. M.; Karuthedath, S.; Liu, W.; Markina, A.; Huang, W.; Chattopadhyay, S.; Nahid, M. M.; Nugraha, M. I.; Lin, Y.; et al. Long-range exciton diffusion in molecular non-fullerene acceptors. *Nat. Commun.* **2020**, *11*, 5220.
(13) Berghuis, A. M.; Raziman, T.; Halpin, A.; Wang, S.; Curto, A. G.; Rivas, J. G. Effective negative diffusion of singlet excitons in organic semiconductors. *J. Phys. Chem. Lett.* **2021**, *12*, 1360−1366.
(14) Wang, R.; Ruzicka, B. A.; Kumar, N.; Bellus, M. Z.; Chiu, H.-Y.; Zhao, H. Ultrafast and spatially resolved studies of charge carriers in atomically thin molybdenum disulfide. *Phys. Rev. B: Condens. Matter Mater. Phys.* **2012**, *86*, 045406.
(15) Cui, Q.; Ceballos, F.; Kumar, N.; Zhao, H. Transient absorption microscopy of monolayer and bulk WSe2. *ACS Nano* **2014**, *8*, 2970−2976.
(16) Davydova, D.; de la Cadena, A.; Akimov, D.; Dietzek, B. Transient absorption microscopy: Advances in chemical imaging of photoinduced dynamics. *Laser Photon. Rev.* **2016**, *10*, 62−81.
(17) Kulig, M.; Zipfel, J.; Nagler, P.; Blanter, S.; Schüller, C.; Korn, T.; Paradiso, N.; Glazov, M. M.; Chernikov, A. Exciton diffusion and halo effects in monolayer semiconductors. *Laser Photon. Rev.* **2018**, *120*, 207401.
(18) Perea-Causin, R.; Brem, S.; Rosati, R.; Jago, R.; Kulig, M.; Ziegler, J. D.; Zipfel, J.; Chernikov, A.; Malic, E. Exciton propagation and halo formation in two-dimensional materials. *Nano Lett.* **2019**, *19*, 7317−7323.
(19) Xiao, X.; Wu, M.; Ni, Z.; Xu, S.; Chen, S.; Hu, J.; Rudd, P. N.; You, W.; Huang, J. Ultrafast exciton transport with a long diffusion length in layered perovskites with organic cation functionalization. *Adv. Mater.* **2020**, *32*, 2004080.
(20) Seitz, M.; Magdaleno, A. J.; Alcázar-Cano, N.; Meléndez, M.; Lubbers, T. J.; Walraven, S. W.; Pakdel, S.; Prada, E.; Delgado-Buscalioni, R.; Prins, F. Exciton diffusion in two-dimensional metal-halide perovskites. *Nat. Commun.* **2020**, *11*, 2035.
(21) Seitz, M.; Meléndez, M.; Alcázar-Cano, N.; Congreve, D. N.; Delgado-Buscalioni, R.; Prins, F. Mapping the Trap-State Landscape in 2D Metal-Halide Perovskites Using Transient Photoluminescence Microscopy. *Adv. Opt. Mater.* **2021**, *9*, 2001875.
(22) Akselrod, G. M.; Prins, F.; Poulikakos, L. V.; Lee, E. M.; Weidman, M. C.; Mork, A. J.; Willard, A. P.; Bulovic, V.; Tisdale, W. A. Subdiffusive exciton transport in quantum dot solids. *Nano Lett.* **2014**, *14*, 3556−3562.
(23) Wittmann, B.; Wiesneth, S.; Motamen, S.; Simon, L.; Serein-Spirau, F.; Reiter, G.; Hildner, R. Energy transport and light propagation mechanisms in organic single crystals. *J. Chem. Phys.* **2020**, *153*, 144202.
(24) Müller, A. M.; Bardeen, C. J. Using a streak camera to resolve the motion of molecular excited states with picosecond time resolution and 150 nm spatial resolution. *J. Phys. Chem. C* **2007**, *111*, 12483−12489.
(25) Ruzicka, B. A.; Werake, L. K.; Samassekou, H.; Zhao, H. Ambipolar diffusion of photoexcited carriers in bulk GaAs. *Appl. Phys. Lett.* **2010**, *97*, 262119.
(26) Mikhnenko, O. V.; Blom, P. W.; Nguyen, T.-Q. Exciton diffusion in organic semiconductors. *Energy Environ. Sci.* **2015**, *8*, 1867−1888.
(27) Tokmoldin, N.; Hosseini, S. M.; Raoufi, M.; Phuong, L. Q.; Sandberg, O. J.; Guan, H.; Zou, Y.; Neher, D.; Shoaee, S. Extraordinarily long diffusion length in PM6: Y6 organic solar cells. *J. Mater. Chem. A* **2020**, *8*, 7854−7860.
(28) Yuan, J.; Zhang, Y.; Zhou, L.; Zhang, G.; Yip, H.-L.; Lau, T.-K.; Lu, X.; Zhu, C.; Peng, H.; Johnson, P. A.; et al. Single-junction

organic solar cell with over 15% efficiency using fused-ring acceptor with electron-deficient core. *Joule* **2019**, *3*, 1140−1151.
(29) Wen, Z.-C.; Yin, H.; Hao, X.-T. Recent progress of PM6: Y6-based high efficiency organic solar cells. *Surface. Interfac.* **2021**, *23*, 100921.
(30) Huang, X.; Vasilev, C.; Hunter, C. N. Excitation energy transfer between monomolecular layers of light harvesting LH2 and LH1-reaction centre complexes printed on a glass substrate. *Lab Chip* **2020**, *20*, 2529−2538.
(31) Qian, P.; Swainsbury, D. J.; Croll, T. I.; Castro-Hartmann, P.; Divitini, G.; Sader, K.; Hunter, C. N. Cryo-EM structure of the Rhodobacter sphaeroides light-harvesting 2 complex at 2.1 Å. *Biochemistry* **2021**, *60*, 3302−3314.
(32) Pflock, T. J.; Oellerich, S.; Krapf, L.; Southall, J.; Cogdell, R. J.; Ullmann, G. M.; Kohler, J. The electronically excited states of LH2 complexes from Rhodopseudomonas acidophila strain 10050 studied by time-resolved spectroscopy and dynamic Monte Carlo simulations. II. Homo-arrays of LH2 complexes reconstituted into phospholipid model membranes. *J. Phys. Chem. B* **2011**, *115*, 8821−8831.
(33) Dahlberg, P. D.; Ting, P.-C.; Massey, S. C.; Allodi, M. A.; Martin, E. C.; Hunter, C. N.; Engel, G. S. Mapping the ultrafast flow of harvested solar energy in living photosynthetic cells. *Nat. Commun.* **2017**, *8*, 988.
(34) Escalante, M.; Lenferink, A.; Zhao, Y.; Tas, N.; Huskens, J.; Hunter, C. N.; Subramaniam, V.; Otto, C. Long-range energy propagation in nanometer arrays of light harvesting antenna complexes. *Nano Lett.* **2010**, *10*, 1450−1457.
(35) Rose, T. S.; Righini, R.; Fayer, M. Picosecond transient grating measurements of singlet exciton transport in anthracene single crystals. *Chem. Phys. Lett.* **1984**, *106*, 13−19.
(36) Eichler, H. J.; Günter, P.; Pohl, D. W. *Laser-Induced Dynamic Gratings*; Springer, 2013; Vol. *50*.
(37) Crank, J. *The Mathematics of Diffusion*; Clarendon−Oxford University Press, 1975.
(38) Tamai, Y.; Ohkita, H.; Benten, H.; Ito, S. Exciton diffusion in conjugated polymers: from fundamental understanding to improvement in photovoltaic conversion efficiency. *J. Phys. Chem. Lett.* **2015**, *6*, 3417−3428.
(39) Xiao, Y.; Yuan, J.; Zhou, G.; Ngan, K. C.; Xia, X.; Zhu, J.; Zou, Y.; Zhao, N.; Zhan, X.; Lu, X. Unveiling the crystalline packing of Y6 in thin films by thermally induced "backbone-on" orientation. *J. Mater. Chem. A* **2021**, *9*, 17030−17038.

https://doi.org/10.1021/acsphotonics.4c00004
ACS Photonics 2024, 11, 1318−1326